Supporting Information:

Co(II) complexes of tetraazamacrocycles appended with amide or hydroxypropyl groups as paraCEST agents

Jaclyn J. Raymond,[a] Samira M. Abozeid,[a‡] Gregory E. Sokolow, [a] Christopher J. Bond, [a] Constance E. Yap,[a] Alexander Y. Nazarenko,[b] Janet R. Morrow [a]

[a] Department of Chemistry, Natural Sciences Complex, University at Buffalo, the State University of New York, Amherst NY 14260

[b] Chemistry Department, SUNY College at Buffalo, 1300 Elmwood Ave, Buffalo NY 14222

‡ Current address: Department of Chemistry, Faculty of Science, Mansoura University, El-Gomhoria Street, 35516 Mansoura, Egypt

Contents

Materials and Methods.

Materials. All reagents and solvents were reagent grade and used as obtained without further purification. 1,4,8,11-tetraazacyclotetradecane (CYCLAM, 98%) and 1,4,7,10-tetraazacyclododecane (CYCLEN, 98%) were purchased from Strem Chemicals. 2-bromoacetamide (98%) was purchased from Acros organics. *S*-(−)-propylene oxide (>98%) and sodium 3-(trimethylsilyl)-1-propanesulfonic acid (TMPS) were purchased from TCI America. Palladium on carbon was purchased from Sigma Aldrich. Cobalt nitrate hexahydrate ($Co(NO_3)_2 \bullet 6H_2O$) was purchased from Fisher Scientific. Cobalt chloride hexahydrate ($CoCl_2 \bullet 6H_2O$) was purchased from Alfa Aesar. N,N-Diisopropylethylamine (DIPEA) (99%) was purchased from BeanTown Chemical.

Crystal Information. For bis[(1,1',1'',1'''-(1,4,7,10-tetraazacyclododecane-1,4,7,10-tetrayl)tetrakis(propan-2-ol))-cobalt(ii)] bis(chloride) tetrachloro-cobalt(ii) acetonitrile solvate hydrate (THP complex) (CCDC 2022193), (1,1'-(1,4,7,10-tetraazacyclododecane-1,7-diyl)bis(propan-2-ol))-cobalt(ii) tetrachloro-cobalt(ii) (DHP complex) (CCDC 2022194), and (2,2'-{4-(2-hydroxypropyl)-10-[2-(hydroxy)propyl]-1,4,7,10-tetraazacyclododecane-1,7-diyl}bis(acetamide))-cobalt(ii) tetrachloro-cobalt(ii) acetonitrile solvate monohydrate (HPAC complex) (CCDC 2022195), single-crystal X-ray data of the complexes were collected on a Bruker VENTURE Photon-100 CMOS diffractometer at 173 K with APEX 2 software suite. The absorption correction was applied using multiscan *SADABS2014*/5 (Bruker,2014/5)[1] and the structures were solved by the direct methods using SHELXT,85 and were refined using the SHELXL-2014 program package. Computer programs: *SAINT* v8.34A (Bruker, 2013),[2] XT (Sheldrick, 2015),[3] XL (Sheldrick, 2008),[4] Olex2 (Dolomanov *et al.*, 2009).[5]

For (4,11-bis(carbamoylmethyl)-1,4,8,11-tetraazacyclotetradecane)-cobalt(ii) dichloro hexahydrate (Co(II) complex of BABC) (CCDC 2262252), single-crystal X-ray diffraction was performed on a Bruker D8 VENTURE Photon-II diffractometer equipped a fixed-chi goniometer, a molybdenum X-ray source (Mo-Kα 0.7107 Å) with a graphite monochromator, and a Photon-100 detector. Crystals were kept at temperature using an Oxford 700 series cryostat cooler. A single crystal was mounted on MiTeGen loop after being suspended in paraffin oil. Data was collected at 113.65 K in using a series of ϕ and ω scans. The structure was solved using Olex2,[5] a graphical user interface. SHELXT,[3] via Intrinsic Phasing was used to solve the structure, which was refined using ShelXL[4] by using a least squares minimization.

NMR Spectroscopy. ^{1}H and ^{13}C NMR spectra were acquired on a Varian 400 MHz or 500 MHz NMR or Bruker 500 NMR at 25^{o}C, unless otherwise stated. Spectra were processed on ACD lab software or with MestReNovax64.

CEST Experiments. CEST data were acquired on a Varian 400 MHz NMR spectrometer with a presaturation pulse power B_1 of 22 μT applied for 2.4 s at 37 °C, unless otherwise stated. Solutions contained 10 mM complex, 20 mM MES or HEPES buffer, and 100 mM NaCl, and at pH values between 5.0 and 8.1. Data were acquired in 1 ppm increments and plotted as normalized

water signal intensity (M_Z/M_0 %) against frequency offset (ppm) to generate CEST spectra. Data was processed and plotted by using Microsoft Excel.

Standardization of the Complexes by ^{1}H NMR. The purity (%) of the complexes was determined by ^{1}H NMR using a Varian 400 MHz NMR spectrometer. The samples contained 20-25 mM of the respective complex and an internal standard using 5-8 mM sodium 3-trimethylsilyl-1-propanesulfonate (TMPS). The experiments were carried out at 25 °C for all of the complexes, except for $[Co(HPAC)]^{2+}$, which was performed at 60 °C to reduce peak width attributed to fluxional processes (see Figure S1). Using the average integration of paramagnetic peaks with respect to the internal standard, the percent purity was calculated using the below equation[6]:

$$\text{wt \% A} = \frac{\text{area under A peak}}{\text{area under IS peak}} \times \frac{\text{MW of A}}{\text{MW of IS}} \times \frac{\text{weight IS}}{\text{weight A}} \times \frac{\text{no. identical } ^1\text{H (IS)}}{\text{no. } ^1\text{H (A)}} \times (\text{purity IS})\%$$

Evans Method for Determination of Magnetic Moments. Evans method was used to determine the effective magnetic moments (μ_{eff}) for the complexes.[7] Three independently measured values were averaged. In a typical experiment, a solution of 10 mM Co(II) complex in water, neutral pH (6-8), containing 5% *tert*-butanol (v/v) was placed in an NMR tube insert, while a reference solution of 5% *tert*-butanol (v/v) in deuterium oxide was contained in the NMR tube. The mass susceptibility χ_g was calculated using Eq. 1 below, where Δf is the shift in frequency (Hz); ν_0 is the operating frequency of NMR spectrometer (Hz); and m is the concentration of the substance (g/mL). The solvent correction (χ_o) was taken into account (Eq. 1). Multiplication of the mass susceptibility by the molar mass yields the molar susceptibility (χ_M). Then the paramagnetic molar susceptibility χ_M^p was calculated from subtracting the diamagnetic susceptibility contribution (χ_M^{dia}) (Eq. 2).[8] This was used to calculate μ_{eff} (Eq. 3).

$$\chi_g = \frac{3\Delta f}{4\pi\nu_0 m} + \chi_o \qquad \text{Eq. 1}$$

$$\chi_M^p = \chi_M - \chi_M^{dia} \qquad \text{Eq. 2}$$

$$\mu_{eff} = 2.83(\chi_M^p T)^{1/2} \qquad \text{Eq. 3}$$

Methods for Monitoring Dissociation of Complexes. UV-vis spectroscopy was used to monitor complex dissociation in the presence of competing cations (excess Zn^{2+}), anions (13 mM CO_3^{2-}, 0.2 mMPO_3^{2-}, and 50 mM Cl^-), and under acidic conditions (2 M HCl or 0.1 M HCl). Samples were incubated at 37 °C and absorbance measurements were recorded over at least 22 hours to monitor the absorption bands corresponding to d-d transitions of the associated complex. For the transmetallation studies, the samples contained a 1:3 ratio of complex to Zn^{2+}. The samples with anions contained 14-20 mM complex, 13 mM K_2CO_3, 0.2 mM Na_2HPO_4, 50 mM NaCl, and 20 mM HEPES buffer at pH = 7.1 or 7.2. For studies in acidic conditions, the absorption bands for $[Co(THP)]^{2+}$ (20 mM) and $[Co(BABC)]^{2+}$ (20 mM) were monitored in 2 M HCl or 0.1 M HCl, respectively.

Synthesis of the Macrocyclic Ligands.

Synthesis of 1,7-bis(2-hydroxypropyl)-1,4,7,10-tetraazacyclododecane (DHP). The precursor to the DHP ligand, 1,7-dibenzyl-1,4,7,10-tetraazacyclododecane (dibenzyl CYCLEN), was prepared by a previously reported method.[9] Dibenzyl CYCLEN (2.65 mmol) was then dissolved in ethanol and to this solution was added N,N-Diisopropylethylamine (DIPEA) (~1 mL) and *S*-(−)-propylene oxide (10.6 mmol, 4 equiv.). The reaction mixture was allowed to stir at room temperature (RT) for 3 days, then the solvent was removed by rotary evaporation to yield a pale-yellow oil that was subjected to hydrogenation with 10 mol % of palladium on carbon (Pd/C) in methanol under H_2 atmosphere in a Parr hydrogenator for three days. The resulting mixture was filtered through celite and concentrated to dryness to obtain DHP (see Scheme S1). The pale-yellow, oily product was then dissolved in methanol and precipitated out as a white solid using ethyl ether. Yield: 79%. ESI-MS *m/z* 291 ($[M+2H^+]^+$, 100%). δH(400 MHz; D_2O; 25 °C) 0.99 (6 H, d, pendant CH_3), 2.28 (4 H, d, pendant CH_2), 2.51 (4 H, d, ring CH_2), 2.63-2.68 (4 H, m, ring C*H*$_2$NH), 3.64-3.69 (2 H, m, pendant CH). δC(400 MHz; D_2O; 25 °C) 20.2 (pendant CH_3), 43.2 (ring CH_2NH), 51.4 (ring CH_2N), 61.6 (pendant CH_2), 65.5 (pendant CH).

Synthesis of 1,7-bis(2-hydroxypropyl)-4,10-bis(carbamoylmethyl)-1,4,7,10-tetraazacyclododecane (HPAC). The precursor ligand DHP (0.4273 g, 1.48 mmol) was dissolved in acetonitrile and stirred at 60 °C with 2-bromoacetamide (3.41 mmol, 2.3 equiv.). After 3 days, the reaction mixture was concentrated to dryness by rotary evaporation to obtain a pale-yellow, oily product that was used without further purification (Scheme S2 below). Yield: 84%. ESI-MS *m/z* 404 ($[M+H^+]^+$, 100%). δH(400 MHz; D_2O; 25 °C) 1.13 (6 H, d, pendant CH_3), 2.87-2.93 (4 H, m, ring CH_2), 3.09-3.14 (4 H, m, ring CH_2), 3.18 (4 H, d, alcohol pendant CH_2), 3.43-3.51 (2 H, m, alcohol pendant CH), 3.80 (4 H, s, amide pendant CH_2). δC(400 MHz; D_2O; 25 °C) 20.2 (pendant CH_3CHOH), 27.6 (pendant CH_3CHOH), 47.6 (ring CH_2N), 49.3 (ring CH_2N), 50.8 (pendant CH_2), 51.4 (pendant CH_2), 55.0 (amide pendant CH_2), 59.6 (pendant CH), 61.6 (pendant CH), 174.9 (amide pendant C=O).

Synthesis of 1,8-bis(benzyl)-4,11-(carbamoylmethyl)-1,4,8,11-tetraazacyclotetradecane (BABC). The precursor ligand dibenzyl CYCLAM (1,8-dibenzyl-1,4,8,11-tetraazacyclo-tetradecane) was prepared according to a previously established procedure.[10] Then dibenzyl CYCLAM (0.5473 g, 1.44 mmol) was dissolved in a minimal amount of ethanol in a 50-mL round-bottom flask, to which the base DIPEA (~1 mL) and 2-bromoacetamide (4 equiv.) were also added. The reaction mixture was allowed to stir overnight at 70 °C, then the resulting white solid product was isolated by vacuum filtration and washed with cold ethanol. See Scheme S3 below. Yield: 61%. ESI-MS *m/z* 496 ($[M+H^+]^+$, 100%), 517 ($[M+Na^+]^+$, 5). δH(400 MHz; DMSO-d_6; 25 °C) 1.60 (4 H, s, ring C*H*$_2$), 2.41-2.54 (16 H, m, ring CH_2N), 2.75 (4 H, s, amide pendant C*H*$_2$), 3.49 (4 H, s, benzyl pendant C*H*$_2$), 7.08 (2 H, s, amide pendant NH_2), 7.21-7.27 (10 H, m, benzyl groups).

***Synthesis of 4,11-bis(carbamoylmethyl)-1,4,8,11-tetraazacyclotetradecane (*BAC)**. The previously prepared BABC ligand (0.44 mmol) was subject to hydrogenation with 10 mol % Pd/C

in methanol for 3 days, then filtered through celite and concentrated to dryness by rotary evaporation to yield bisamide cyclam (BAC) (Scheme S4 below). Yield: 88%. ESI-MS *m/z* 158 ($[M/2]^{2+}$, 25%), 315 ($[M+H^+]^+$, 100), 337 ($[M+Na^+]^+$, 16). δH(400 MHz; MeOD-d_4; 25 °C) 1.70-1.75 (4 H, m, macrocycle CH_2), 2.61-2.75 (16 H, m, macrocycle CH_2), 3.10 (4 H, s, pendant CH_2). δC(400 MHz; MeOD-d_4; 25 °C) 21.5 (ring CH_2), 22.8 (ring CH_2), 43.7 (ring CH_2N), 48.8 (ring CH_2N), 49.4 (ring CH_2N), 55.1 (pendant CH_2), 56.5, (pendant CH_2), 174.0 (pendant C=O), 177.1 (pendant C=O).

***Synthesis of 1,8-bis(propan-2-ol)-4,11-(carbamoylmethyl)-1,4,8,11-tetraazacyclotetradecane (*HPAM).** To an ethanolic solution of the resulting ligand BAC (0.58 mmol) was added *S*-(−)-propylene oxide (7 equiv.) and DIPEA. The reaction mixture was allowed to stir at 70 °C for 3 days (Scheme S4 below). Upon cooling, the product was observed as a solid white precipitate, which was then isolated by centrifugation and washed with cold ethanol. Yield: 83%. ESI-MS *m/z* 431 ($[M+H^+]^+$, 100%). δH(400 MHz; DMSO-d_6; 25 °C) 0.98-1.05 (6 H, m, alcohol pendant CH_3), 1.49-1.56 (4 H, m, macrocycle CH_2), 2.16-2.26 (4 H, m, macrocycle CH_2N), 2.79-2.97 (4 H, m, alcohol pendant CH_2), 3.29 (4 H, s, amide pendant CH_2), 3.63 (2 H, s, alcohol pendant CH), 4.40 (2 H, s, pendant O*H*), 7.07 (2 H, s, amide pendant NH_2), 7.31 (2 H, s, amide pendant NH_2). δC(400 MHz; DMSO-d_6; 50 °C) 21.8 (alcohol pendant CH_3), 25.0 (macrocycle CH_2), 51.6, 51.9, 52.7, 53.0 (macrocycle CH_2N), 59.2 (amide pendant CH_2), 62.6 (alcohol pendant CH_2), 64.4 (alcohol pendant CH), 173.5 (amide C=O).

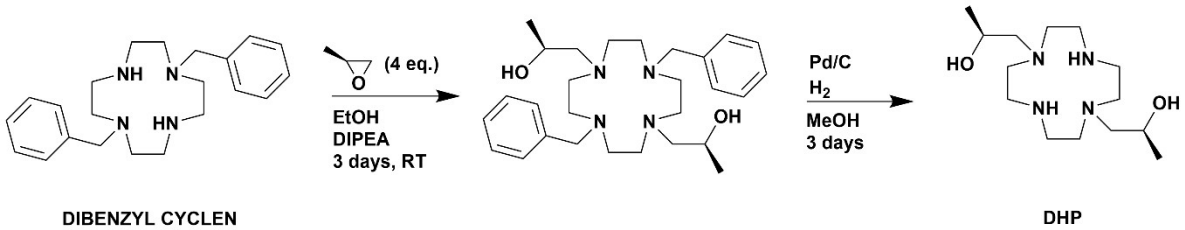

Scheme S1. Synthetic scheme for the DHP ligand.

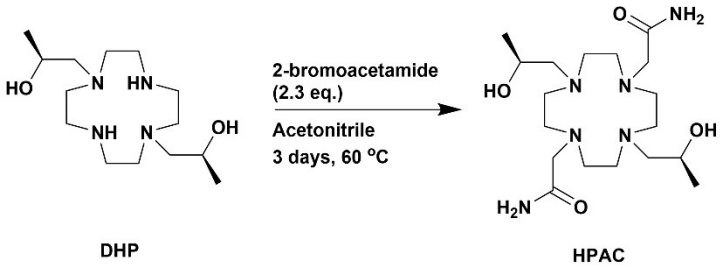

Scheme S2. Synthetic scheme for the HPAC ligand.

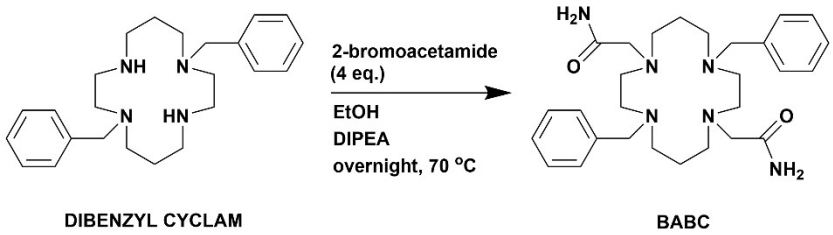

Scheme S3. Synthetic scheme for the BABC ligand.

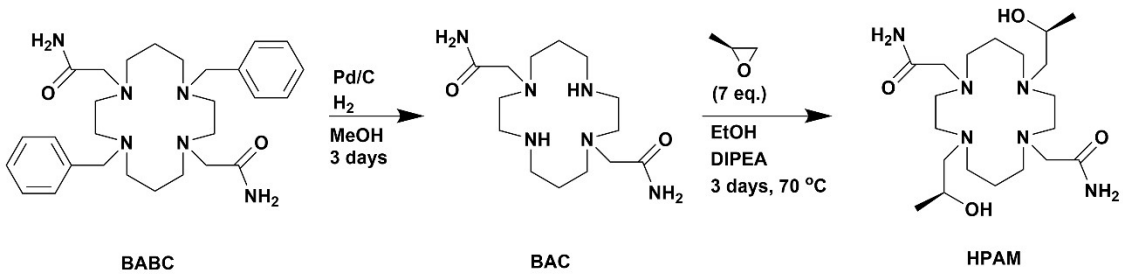

Scheme S4. Synthetic scheme for the HPAM ligand and the precursor ligand BAC.

Synthesis of Cobalt(II) Complexes.

Synthesis of [Co(THP)](NO$_3$)$_2$. The ligand THP (0.3547 g, 0.877 mmol) was dissolved in ethanol in a 25-mL round-bottom flask, to which an ethanolic solution of cobalt nitrate hexahydrate (0.2564 g, 0.881 mmol) was then added (Scheme S5). The reaction mixture was allowed to stir overnight under Argon at RT. The volume was reduced to approximately 3 mL by rotary evaporation, then ethyl ether was added to the solution to induce precipitation of the complex. Upon centrifugation of the resulting mixture, the pink solid product was washed twice with ethyl ether. Yield: 86%. ESI-MS *m/z* 232.00 ([M/2]$^{2+}$, 100%) 462.42 ([M-H$^+$]$^+$, 80), where M = complex cation. Purity: 94% by ^{1}H NMR integration against sodium 3-(trimethylsilyl)-1-propanesulfonic acid (TMPS) standard.

The complexes [Co(DHP)](NO$_3$)$_2$, [Co(HPAC)](NO$_3$)$_2$, [Co(BABC)](NO$_3$)$_2$, and [Co(HPAM)](NO$_3$)$_2$ were prepared similarly as above. See Scheme S5.

[Co(DHP)](NO$_3$)$_2$ **:** Yield: 67%. ESI-MS *m/z* 173.84 ([M/2]$^{2+}$, 58%), 346.32 ([M-H$^+$]$^+$, 100), where M = complex cation**.** Purity: 91% by ^{1}H NMR integration against TMPS standard.

[Co(HPAC)](NO$_3$)$_2$**:** Yield: 80%. ESI-MS *m/z* 230.92 ([M/2]$^{2+}$, 100%), 460.44 ([M-H$^+$]$^+$, 20), where M = complex cation. Purity: 90% by ^{1}H NMR integration against TMPS standard.

[Co(BABC)](NO$_3$)$_2$**:** Yield: 71%. ESI-MS *m/z* 276.84 ([M/2]$^{2+}$, 100%), 552.36 ([M-H$^+$]$^+$, 5), where M = complex cation. Purity: 92% by ^{1}H NMR integration against TMPS standard.

[Co(HPAM)](NO$_3$)$_2$**:** Yield: 66%. ESI-MS *m/z* 244.60 ([M/2]$^{2+}$, 100%), 488.24 ([M-H$^+$]$^+$, 10), where M = complex cation. Purity: 87% by ^{1}H NMR integration against TMPS standard.

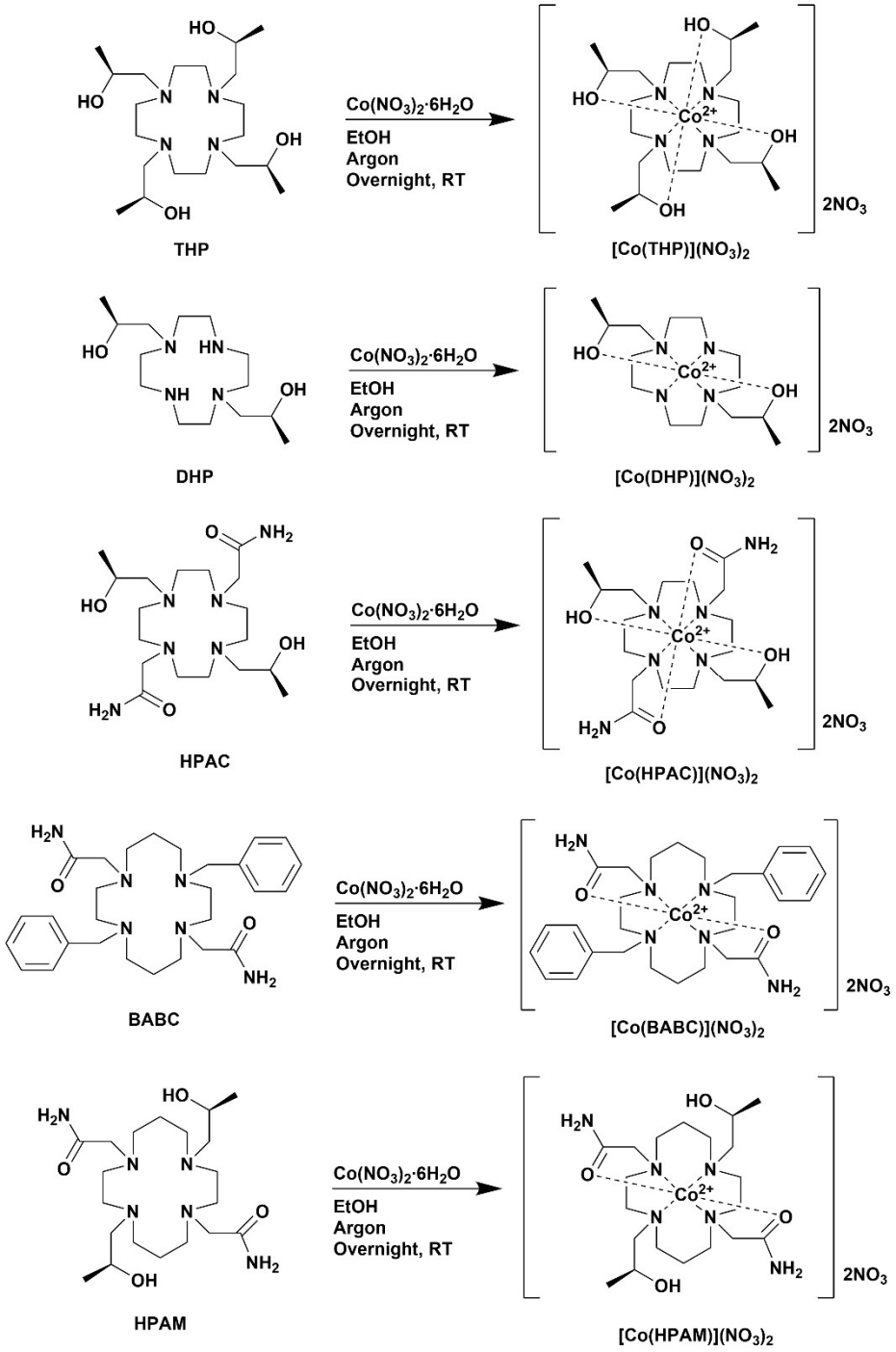

Scheme S5. Synthetic schemes for $[Co(THP)](NO_3)_2$, $[Co(DHP)](NO_3)_2$, $[Co(HPAC)](NO_3)_2$, $[Co(BABC)](NO_3)_2$, and $[Co(HPAM)](NO_3)_2$.

^{1}H NMR Spectra of the Complexes.

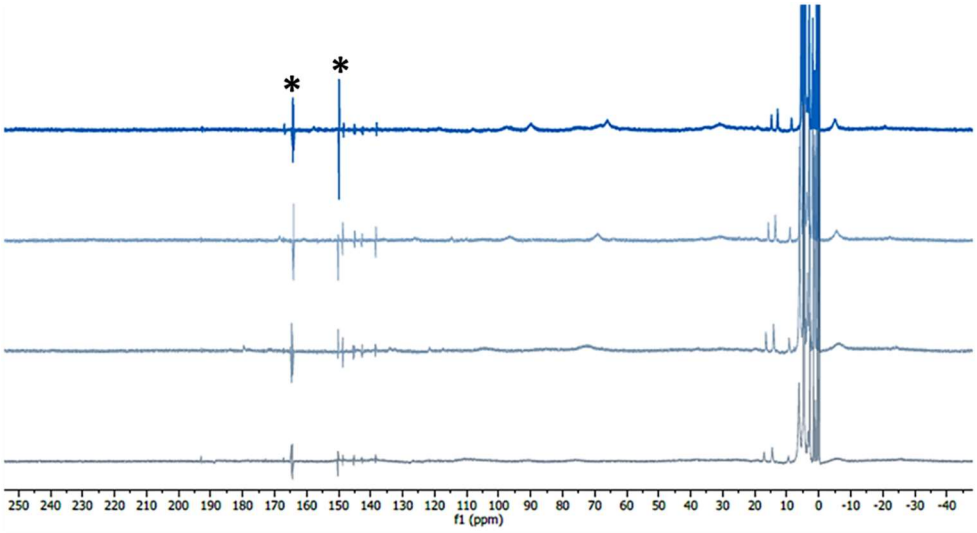

Figure S1. Stacked ^{1}H NMR spectra of $[Co(HPAC)]^{2+}$ (20 mM) in D_2O at various temperatures, T = 25, 40, 60, and 80 °C (bottom to top, respectively). The asterisks indicate artifacts from the spectrometer.

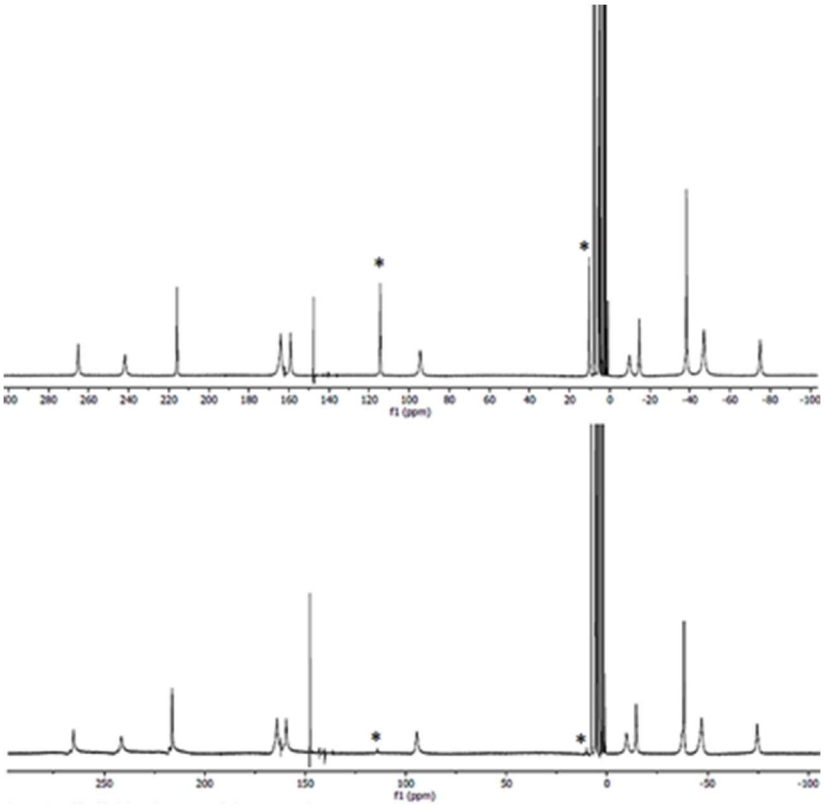

Figure S2. ^{1}H NMR spectra of $[Co(BABC)]^{2+}$ (20 mM) in DMSO (top) and after the addition of D_2O (bottom). The asterisks indicate the proton resonances with reduced signal intensity upon addition of D_2O.

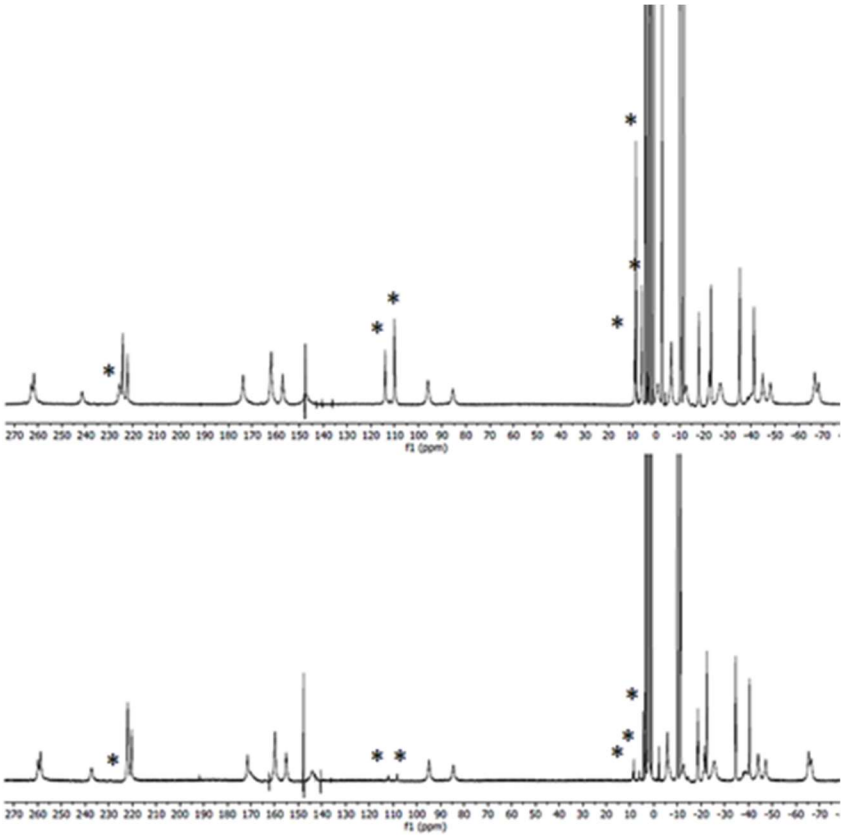

Figure S3. ^{1}H NMR spectra of $[Co(HPAM)]^{2+}$ (20 mM) in DMSO (top) and after the addition of D_2O (bottom). The asterisks indicate the proton resonances with reduced signal intensity upon addition of D_2O.

CEST Spectra.

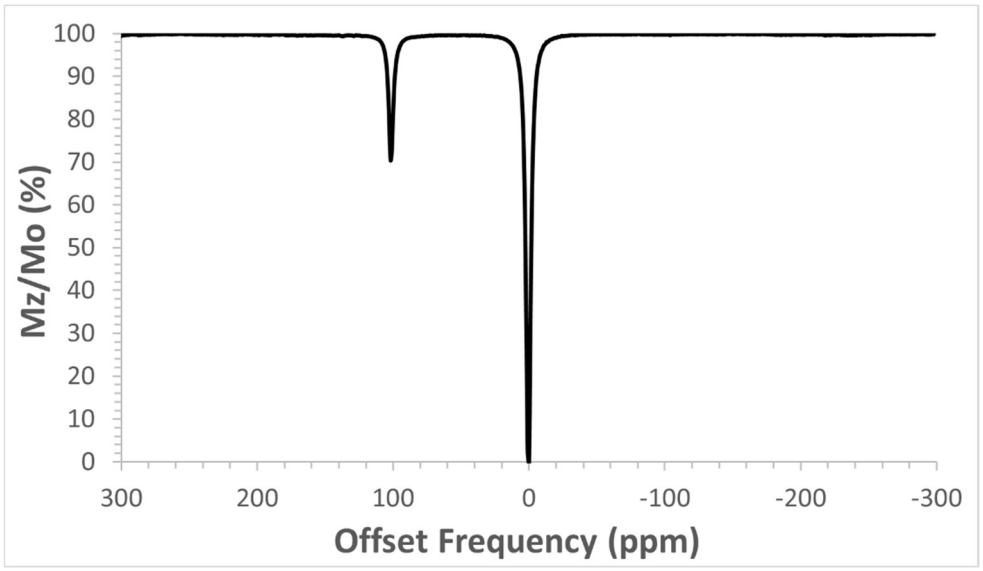

Figure S4. CEST spectrum for $[Co(BABC)]^{2+}$ at pH = 7.3 and T = 37 °C. The sample contained 10 mM complex, 100 mM NaCl, and 20 mM HEPES buffer. B_1 = 22 μT, applied for 2.4 seconds.

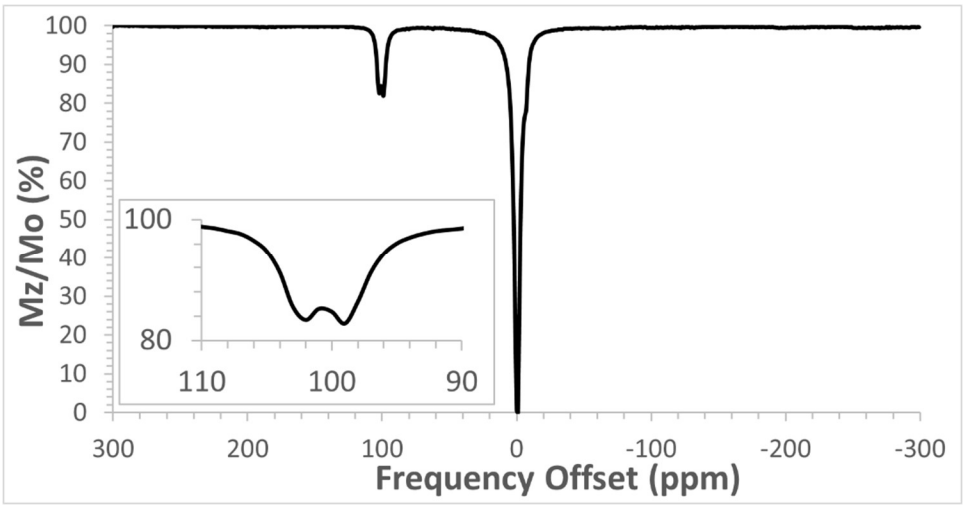

Figure S5. CEST spectrum for $[Co(HPAM)]^{2+}$ at pH = 7.4 and T = 37 °C. The sample contained 10 mM complex, 100 mM NaCl, and 20 mM HEPES buffer. B_1 = 22 µT, applied for 2.4 seconds.

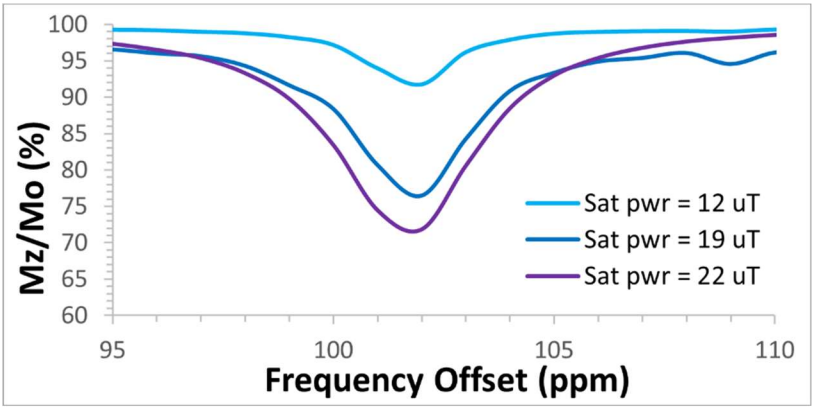

Figure S6. Regional CEST spectra overlay at various saturation power values (12, 19, and 22 µT) for $[Co(BABC)]^{2+}$ (10 mM) at pH = 7.3 and T = 37 °C. The radiofrequency pulse was applied for 2.4 seconds.

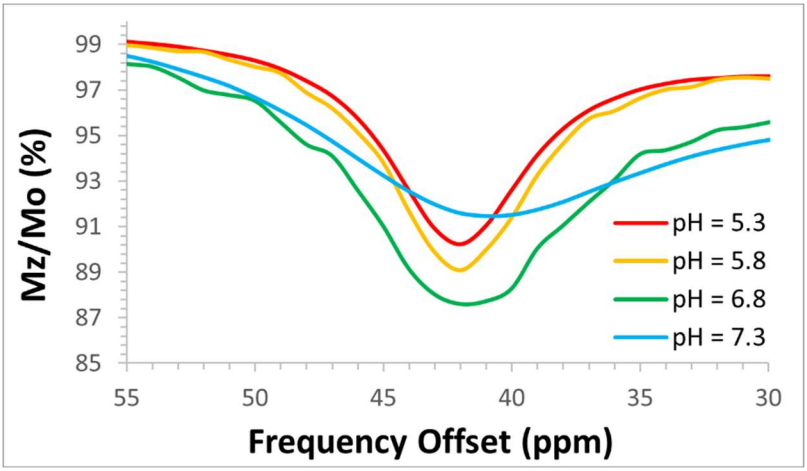

Figure S7. % CEST pH-dependence of the CEST peak at 42 ppm for $[Co(THP)]^{2+}$ at 37 °C. Samples contained 10 mM $[Co(THP)]^{2+}$, 20 mM MES buffer, and 100 mM NaCl. B_1 = 24 µT applied for 2 s.

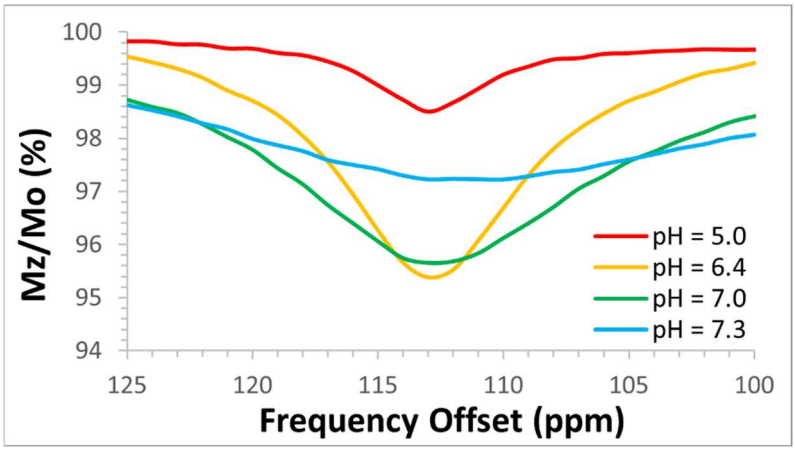

Figure S8. % CEST pH-dependence of the CEST peak at 113 ppm for $[Co(DHP)]^{2+}$ at 37 °C. Samples contained 10 mM $[Co(DHP)]^{2+}$, 20 mM buffer MES, and 100 mM NaCl. B_1 = 24 µT applied for 2 s.

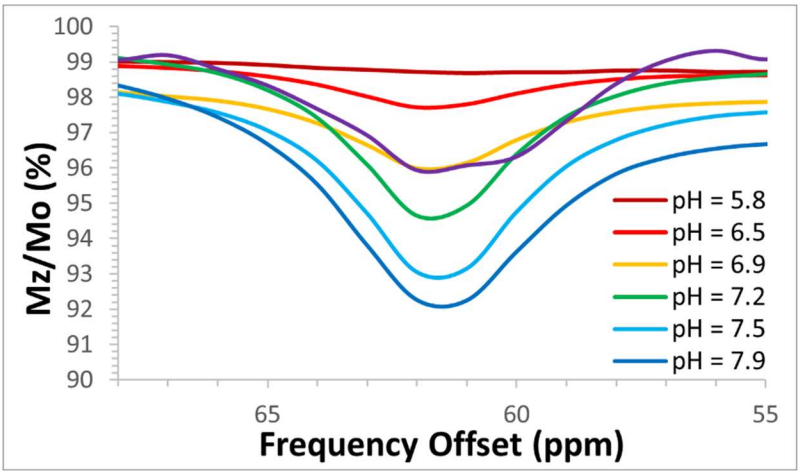

Figure S9. % CEST pH-dependence of the CEST peak at 62 ppm for $[Co(HPAC)]^{2+}$ at 37 °C. Samples contained 10 mM $[Co(HPAC)]^{2+}$, 20 mM buffer MES, 100 mM NaCl. B_1 = 24 µT applied for 2 s.

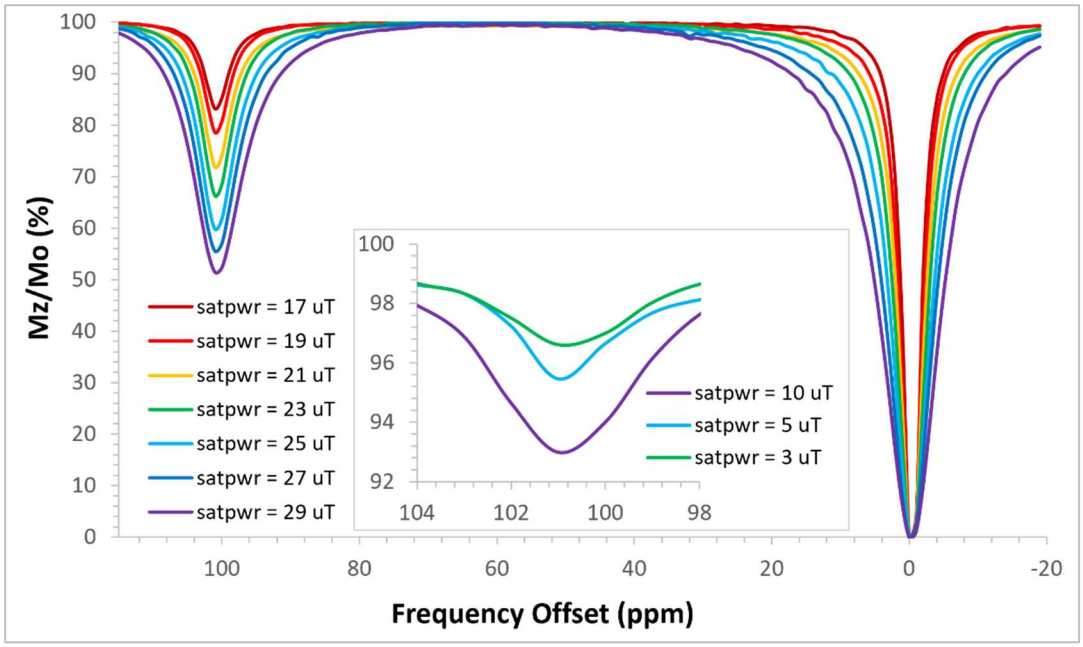

Figure S10. CEST spectra overlay at various saturation power values (19, 21, 23, 25, 27, and 29 µT) for $[Co(BABC)]^{2+}$ at pH = 7.4 and T = 37 °C. The inset contains the respective peak at 3, 5, and 10 µT. Samples contained 10 mM complex, 20 mM HEPES buffer, and 100 mM NaCl. The radiofrequency pulse was applied for 2.4 seconds.

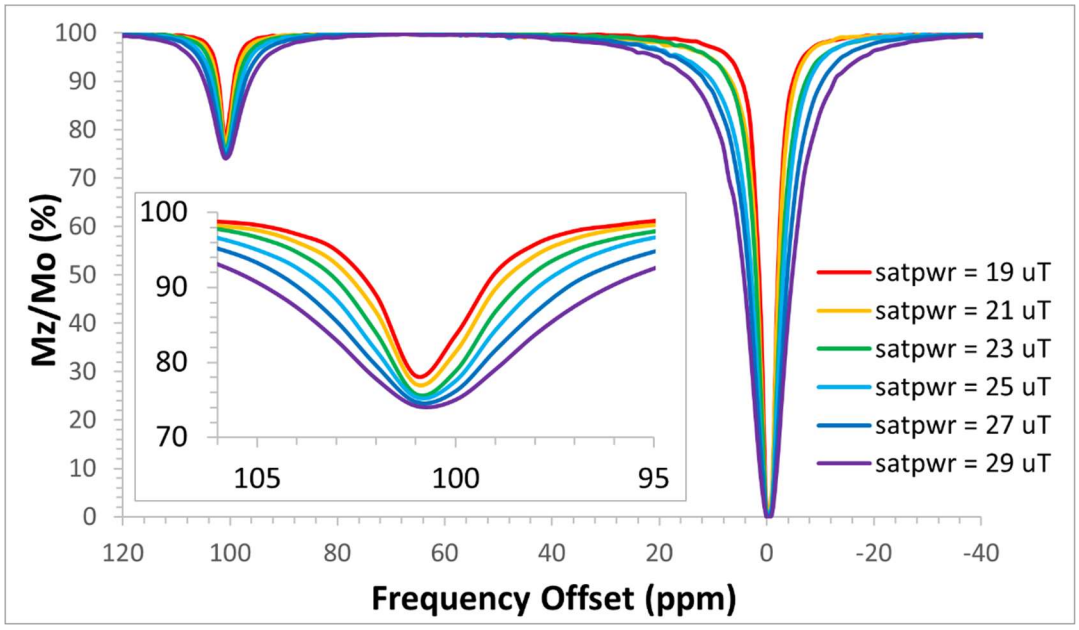

Figure S11. CEST spectra overlay at various saturation power values (19, 21, 23, 25, 27, and 29 µT) for $[Co(BABC)]^{2+}$ at pH = 7.2 and T = 37 °C. Samples contained 10 mM complex, 20 mM HEPES buffer, and 100 mM NaCl. The radiofrequency pulse was applied for 2.4 seconds.

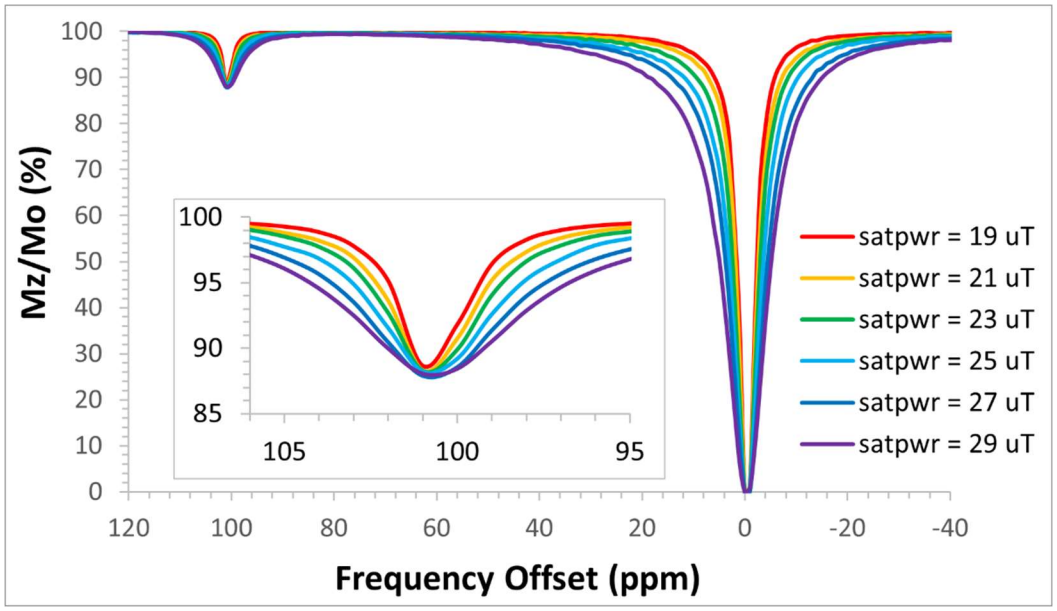

Figure S12. CEST spectra overlay at various saturation power values (19, 21, 23, 25, 27, and 29 µT) for $[Co(BABC)]^{2+}$ at pH = 6.8 and T = 37 °C. Samples contained 10 mM complex, 20 mM HEPES buffer, and 100 mM NaCl. The radiofrequency pulse was applied for 2.4 seconds.

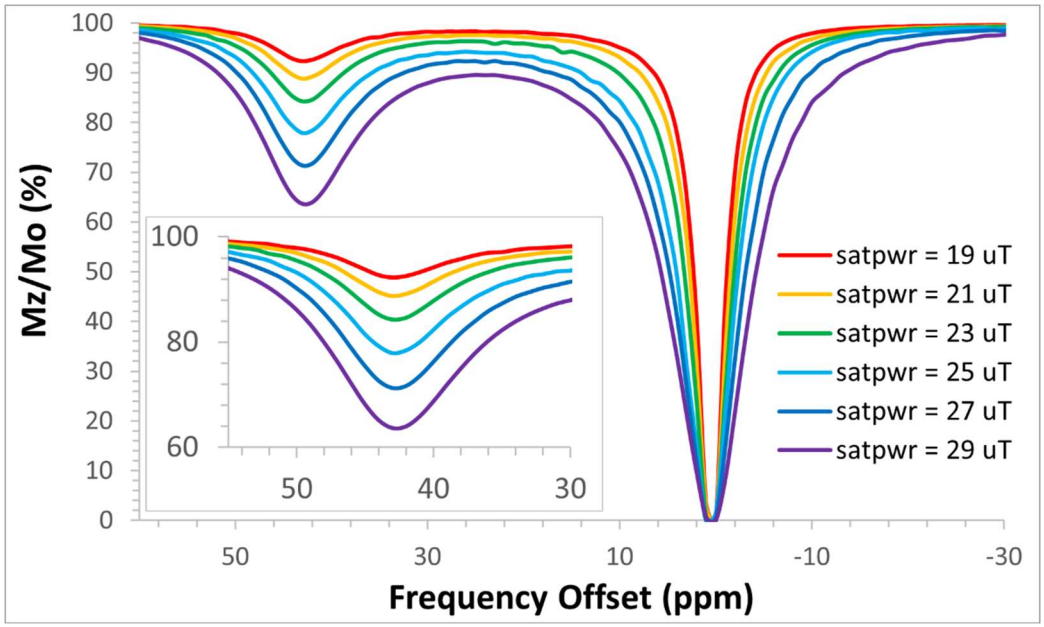

Figure S13. CEST spectra overlay at various saturation power values (19, 21, 23, 25, 27, and 29 µT) for $[Co(THP)]^{2+}$ at pH = 6.8 and T = 37 °C. Samples contained 10 mM complex, 20 mM HEPES buffer, and 100 mM NaCl. The radiofrequency pulse was applied for 2.4 seconds.

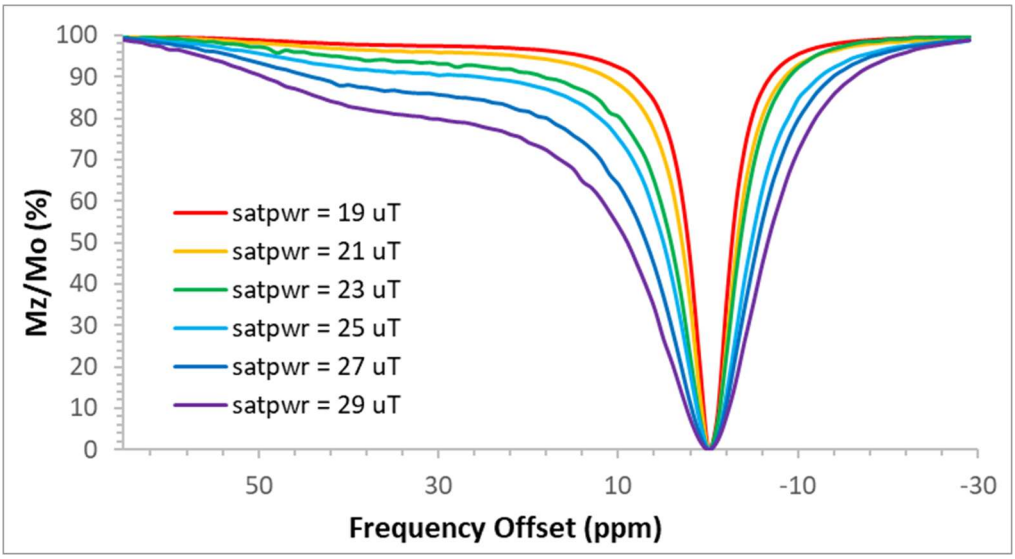

Figure S14. CEST spectra overlay at various saturation power values (19, 21, 23, 25, 27, and 29 µT) for $[Co(THP)]^{2+}$ at pH = 7.4 and T = 37 °C. Samples contained 20 mM complex, 20 mM HEPES buffer, and 100 mM NaCl. The radiofrequency pulse was applied for 2.4 seconds.

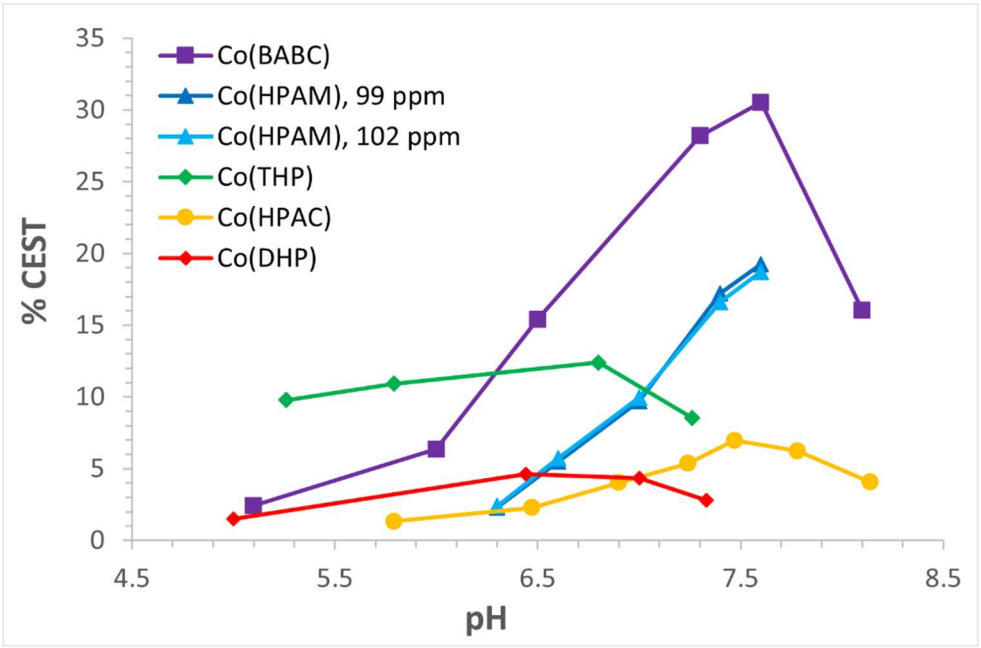

Figure S15. % CEST pH-dependence of the CEST peak(s) intensity for the respective complexes at 37 °C. Samples contained 10 mM complex, 20 mM HEPES buffer, and 100 mM NaCl.

Exchange Rate Constants and Omega Plots.

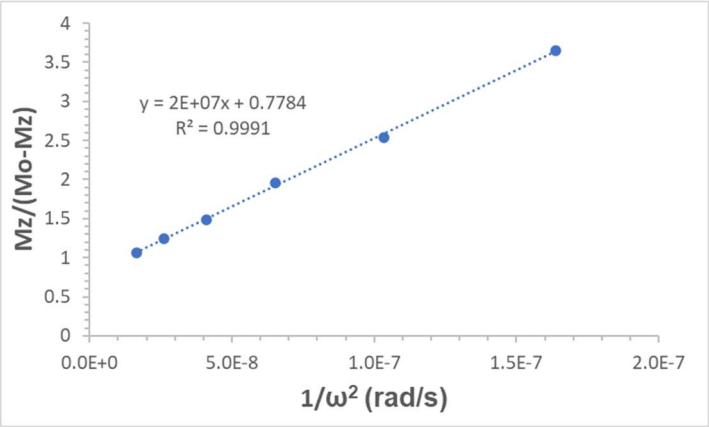

Figure S16. Omega plot for $[Co(BABC)]^{2+}$ at pH = 7.4 and T = 37 °C. k_{ex} was determined to be 4740 s^{-1}. B_1 was varied between 19 and 29 µT.

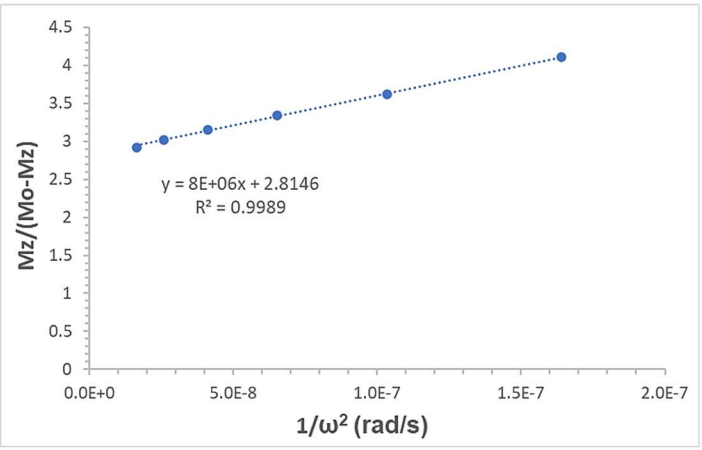

Figure S17. Omega plot for $[Co(BABC)]^{2+}$ at pH = 7.2 and T = 37 °C. k_{ex} was determined to be 1670 s^{-1}. B_1 was varied between 19 and 29 µT.

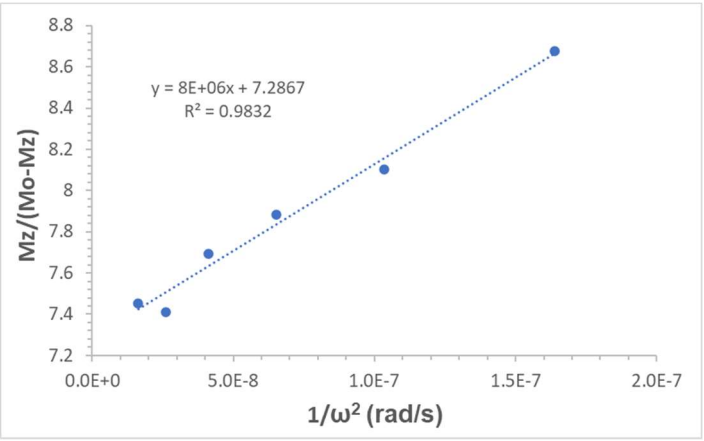

Figure S18. Omega plot for $[Co(BABC)]^{2+}$ at pH = 6.8 and T = 37 °C. k_{ex} was determined to be 1070 s^{-1}. B_1 was varied between 19 and 29 µT.

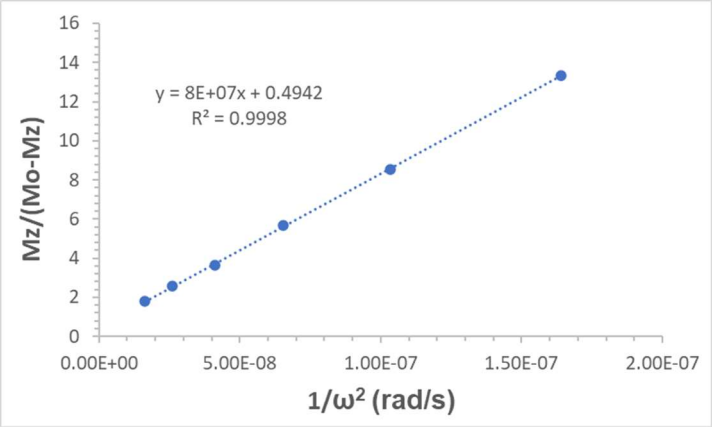

Figure S19. Omega plot for $[Co(THP)]^{2+}$ at pH = 6.8 and T = 37 °C. k_{ex} was determined to be 12600 s^{-1}. B_1 was varied between 19 and 29 μT.

Table S1. Values for k_{ex} at pH 6.8, 7.2, or 7.4 and T = 37 °C for $[Co(BABC)]^{2+}$ (10 mM) or $[Co(THP)]^{2+}$ (10 mM).

Complex	**k_{ex} (s^{-1}) at pH 6.8**	**k_{ex} (s^{-1}) at pH = 7.2**	**k_{ex} (s^{-1}) at pH = 7.4**
$[Co(BABBC)]^{2+}$	1070	1670	4740
$[Co(THP)]^{2+}$	12600	--	--

UV-vis Spectra.

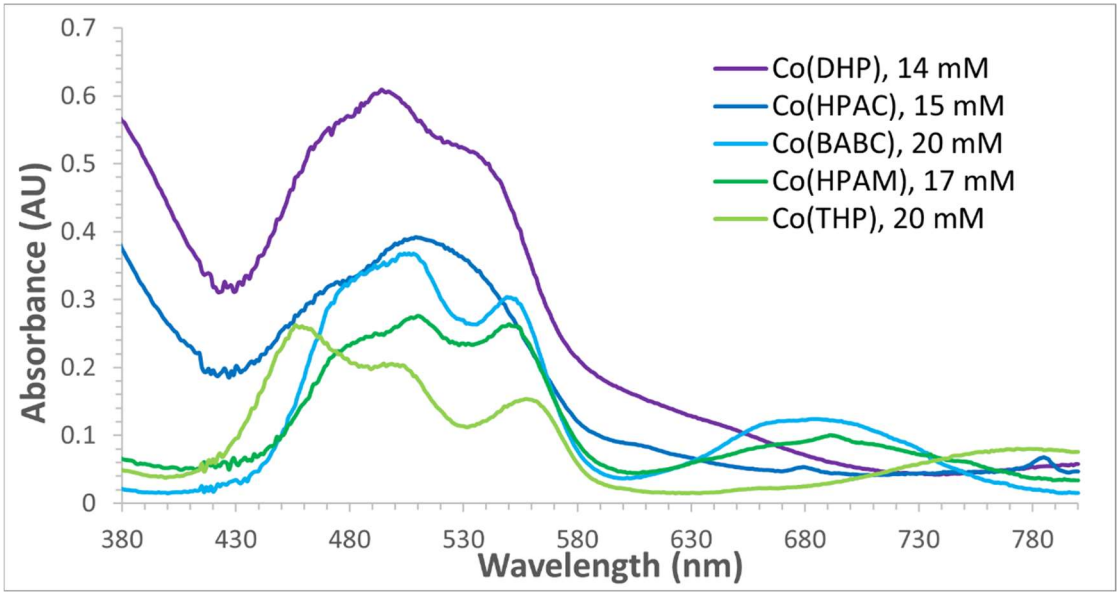

Figure S20. Overlay of the absorbance spectra for the Co(II) complexes. Samples contained aqueous solutions of the respective complex (14-20 mM).

***Table S2*.** Molar Absorptivity (ε) Values for the CYCLEN-based Complexes at the Respective Wavelength (λ) or Wavenumber (*v*).

$[Co(THP)]^{2+}$			$[Co(DHP)]^{2+}$			$[Co(HPAC)]^{2+}$		
λ (nm)	***v*** **(cm^{-1})**	**ε (M^{-1} cm^{-1})**	**λ (nm)**	***v*** **(cm^{-1})**	**ε (M^{-1} cm^{-1})**	**λ (nm)**	***v*** **(cm^{-1})**	**ε (M^{-1} cm^{-1})**
456	21930	13	470	21277	40	~467	21413	20.7
499	20040	10	494	20243	45	509	19646	26.1
557	17953	8	541	18484	37	--	--	--

***Table S3*.** Molar Absorptivity (ε) Values for the CYCLAM-based Complexes at the Respective Wavelength (λ) or Wavenumber (*v*).

$[Co(BABC)]^{2+}$			$[Co(HPAM)]^{2+}$		
λ (nm)	***v*** **(cm^{-1})**	**ε (M^{-1} cm^{-1})**	**λ (nm)**	***v*** **(cm^{-1})**	**ε (M^{-1} cm^{-1})**
~478	20921	16.2	479	20877	13.6
506	19763	18.4	510	19608	16.2
549	18215	16.2	550	18182	15.5

Complex Dissociation Studies.

Zn^{2+} ion displacement

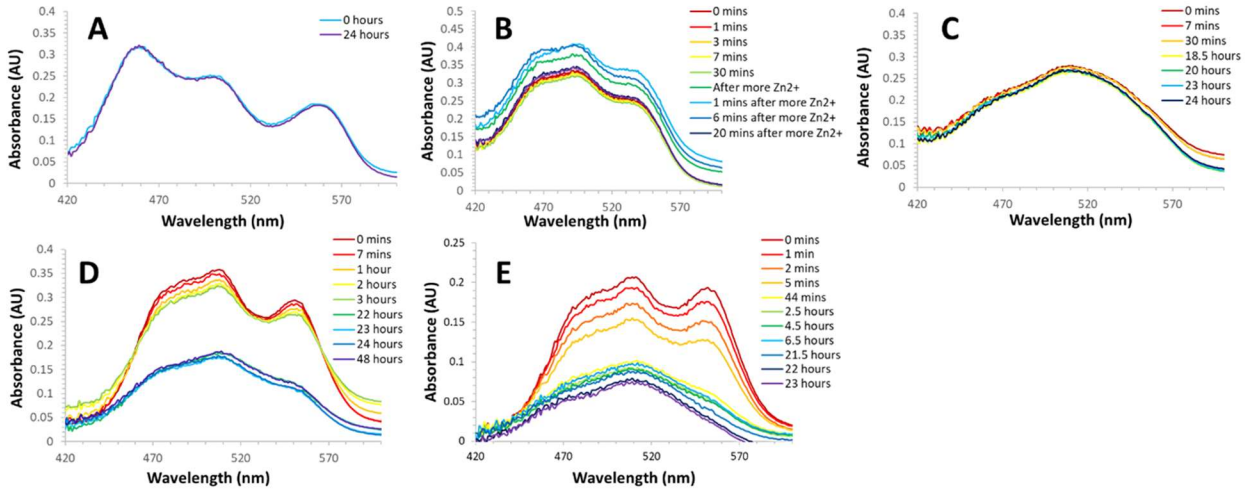

Figure S21. Absorbance spectra overlay for 20 mM $[Co(THP)]^{2+}$ (A), 14 mM $[Co(DHP]^{2+}$ (B), 20 mM $[Co(HPAC)]^{2+}$ (C), 20 mM $[Co(BABC)]^{2+}$ (D), and 17 mM $[Co(HPAM)]^{2+}$ (E) in the presence of excess Zn^{2+} (1:3 or 1:4.3 complex to zinc ratio). Samples contained a ratio of 1:3 complex to zinc at T = 37.0°C.

Dissociation in the presence of acid or anions.

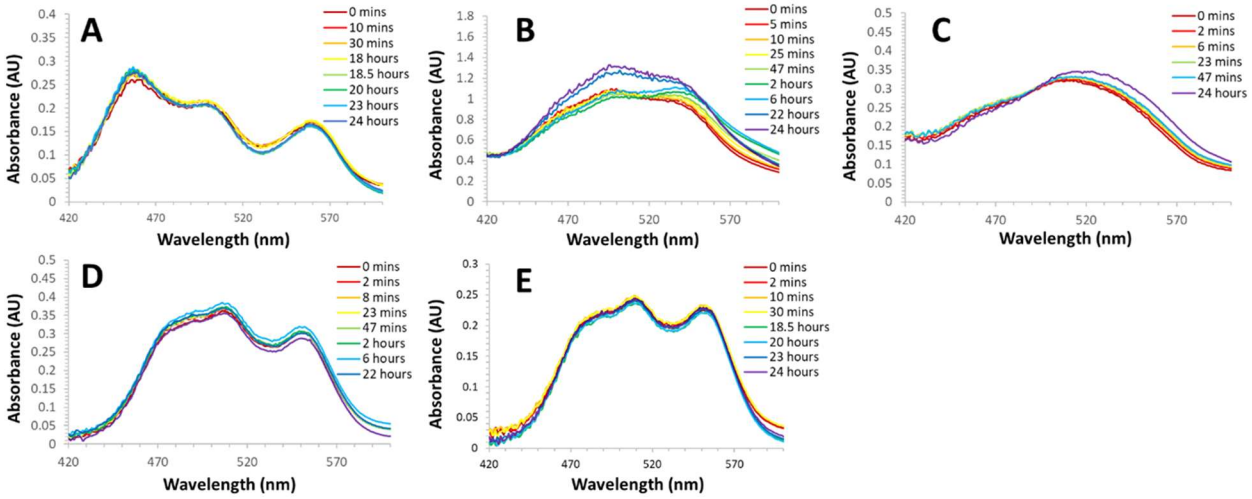

Figure S22. Absorbance spectra overlay 20 mM $[Co(THP)]^{2+}$ (A), 14 mM $[Co(DHP]^{2+}$ (B), 20 mM $[Co(HPAC)]^{2+}$ (C), 20 mM $[Co(BABC)]^{2+}$ (D), and 17 mM $[Co(HPAM)]^{2+}$ (E) in the presence of biologically-relevant anions. Samples contained 0.2 mM Na_2HPO_4, 13 mM K_2CO_3, 50 mM NaCl, and 20 mM HEPES buffer at pH = 7.1 or 7.2 and T = 37.0°C.

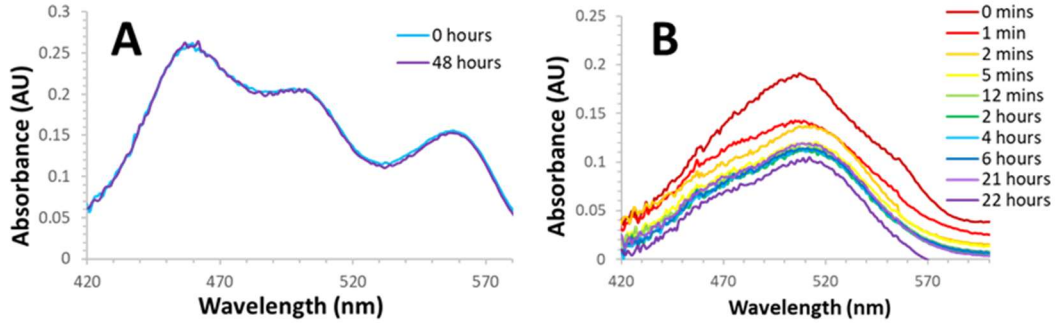

Figure S23. Absorbance spectra overlay for 20 mM $[Co(THP)]^{2+}$ (A) in the presence of 2 M HCl and 20 mM $[Co(BABC)]^{2+}$ (B) in 0.1 M HCl at T = 37 °C.

Crystallographic Data.

Table S4. Crystal data, data collection and structure refinement details for the Co(II) complexes.

Compound	HPAC Complex CCDC 2022195	DHP Complex CCDC 2022194	THP Complex CCDC 2022193	BABC Complex CCDC 2262252
Chemical formula	$2(C_{18}H_{38}CoN_6O_4)\cdot 2(Cl_4Co)\cdot 2(H_2O)\cdot 2(C_2H_3N)$	$C_{14}H_{32}CoN_4O_2\cdot Cl_4Co$	$2(C_{20}H_{44}CoN_4O_4)\cdot 2(Cl)\cdot Cl_4Co\cdot 1.69(H_2O)\cdot C_2H_3N$	$[C_{28}H_{42}CoN_6O_2]Cl_2\cdot 6H_2O$
M_r	1442.54	548.09	1270.39	732.60
Crystal system, space group	Orthorhombic, $P2_12_12_1$	Orthorhombic, $P2_12_12_1$	Triclinic, $P1$	Monoclinic, $P2_1/n$
Temperature (K)	173	173	173	114
a, b, c (Å)	16.8813 (8), 18.4751 (9), 20.4087 (10)	10.8000 (9), 13.7390 (14), 15.4056 (15)	9.3476 (7), 10.4026 (7), 15.7740 (11)	10.9214(7), 22.7525(13), 14.3494(9)
α, β, γ (°)	90, 90, 90	90, 90, 90	76.878 (2), 78.518 (2), 89.593 (2)	90, 96.926(2), 90
V (Å^3)	6365.1 (5)	2285.9 (4)	1462.74 (18)	3539.7(4)
Z	4	4	1	4
Radiation type	Mo $K\alpha$	Mo $K\alpha$	Mo $K\alpha$	Mo $K\alpha$ (λ = 0.71073)
μ (mm^{-1})	1.42	1.94	1.17	0.689
Crystal size (mm)	0.59 × 0.26 × 0.15	0.50 × 0.17 × 0.16	0.30 × 0.24 × 0.07	0.175 x 0.15 x 0.1
Data collection				
Diffractometer	Bruker PHOTON-100 CMOS	Bruker PHOTON-100 CMOS	Bruker PHOTON-100 CMOS	Bruker PHOTON-II
Absorption correction	Multi-scan *SADABS2014*/5 (Bruker,2014/5) was used for absorption correction. wR2(int) was 0.0675 before and 0.0624 after correction. The Ratio of minimum to maximum transmission is 0.6566.	Multi-scan *SADABS2016*/2 (Bruker, 2016/2) was used for absorption correction. wR2(int) was 0.0854 before and 0.0676 after correction. The Ratio of minimum to maximum transmission is 0.7803.	Multi-scan *SADABS2014*/5 (Bruker,2014/5) was used for absorption correction. wR2(int) was 0.0556 before and 0.0494 after correction. The Ratio of minimum to maximum transmission is 0.8090.	Multi-scan *SADABS-2016/2* (Bruker,2016/2) was used for absorption correction. wR2(int) was 0.0644 before and 0.0508 after correction. The Ratio of minimum to maximum transmission is 0.9044.
T_{min}, T_{max}	0.546, 0.831	0.582, 0.746	0.769, 0.950	0.886, 0.933
No. of measured, independent and observed [$I > 2\sigma(I)$] reflections	447993, 23270, 19437	42350, 4662, 3809	68318, 10954, 8409	85756, 10903

R_{int}	0.047	0.085	0.070	0.0352
$(\sin\theta/\lambda)_{max}$ (Å^{-1})	0.760	0.625	0.611	0.710
Refinement				
$R[F^2 > 2\sigma(F^2)]$, $wR(F^2)$, S	0.035, 0.088, 1.03	0.031, 0.057, 1.07	0.035, 0.072, 1.04	0.0334, 0.0815, 1.057
No. of reflections	23270	4662	10954	85756
No. of parameters	816	243	704	438
No. of restraints	504	2	10	0
H-atom treatment	H atoms treated by a mixture of independent and constrained refinement	H atoms treated by a mixture of independent and constrained refinement	H atoms treated by a mixture of independent and constrained refinement	H atoms were treated using the riding model.
$\Delta\rangle_{max}$, $\Delta\rangle_{min}$ (e Å^{-3})	0.69, -0.54	0.68, -0.46	0.43, -0.60	0.79, -0.77
Absolute structure	Flack x determined using 8004 quotients [(I+)-(I-)]/[(I+)+(I-)] (Parsons, Flack and Wagner, Acta Cryst. B69 (2013) 249-259)[11].	Flack x determined using 1453 quotients [(I+)-(I-)]/[(I+)+(I-)] (Parsons, Flack and Wagner, Acta Cryst. B69 (2013) 249-259)[11].	Flack x determined using 3558 quotients [(I+)-(I-)]/[(I+)+(I-)] (Parsons, Flack and Wagner, Acta Cryst. B69 (2013) 249-259)[11].	N/A
Absolute structure parameter	-0.005 (2)	-0.036 (8)	-0.001 (5)	N/A

Computer programs: *APEX2* (Bruker, 2013), *SAINT* v8.34A (Bruker, 2013), *SAINT* V8.38A (Bruker, 2016), ShelXT (Sheldrick, 2015)[3], *SHELXL* (Sheldrick, 2015)[4], Olex2 (Dolomanov *et al.*, 2009)[5].

Table S5. Selected bond lengths (Å) for the complex cation $[Co(HPAC)]^{2+}$

Co1—O1	2.153 (2)	Co1—N2	2.317 (2)
Co1—O2	2.186 (2)	Co1—N3	2.271 (3)
Co1—O3	2.164 (2)	Co1—N4	2.328 (3)
Co1—N1	2.237 (3)		

Table S6. Selected bond lengths (Å) for the complex cation $[Co(DHP)]^{2+}$

Co1—O1	2.107 (3)	Co1—N2	2.121 (3)
Co1—O2	2.140 (3)	Co1—N3	2.240 (3)
Co1—N1	2.236 (3)	Co1—N4	2.125 (3)

Table S7. Selected bond lengths (Å) for the complex cation $[Co(THP)]^{2+}$

Co1—O1	2.171 (4)	Co2—O5	2.223 (4)
Co1—O2	2.292 (4)	Co2—O6	2.228 (4)

Co1—O3	2.196 (4)	Co2—O7	2.196 (4)
Co1—N1	2.225 (4)	Co2—N5	2.204 (4)
Co1—N2	2.340 (4)	Co2—N6	2.355 (4)
Co1—N3	2.223 (4)	Co2—N7	2.221 (4)
Co1—N4	2.318 (4)	Co2—N8	2.305 (4)

Table S8. Selected bond lengths (Å) for the complex cation $[Co(BABC)]^{2+}$

Co1—O1	2.095 (1)	Co1—N3	2.286 (2)
Co1—O2	2.096 (1)	Co1—N1	2.244 (1)
Co1—N4	2.226 (1)		
Co1—N2	2.210 (1)		

Table S9. Selected bond angles (°) for the complex cation $[Co(HPAC)]^{2+}$

Atom 1	Atom 2	Atom 3	Angle (°)
O1	Co1	O2	80.41(8)
O1	Co1	O3	80.16(8)
O1	Co1	N1	156.42(9)
O1	Co1	N2	123.83(9)
O1	Co1	N3	73.73(9)
O1	Co1	N4	92.06(9)
O2	Co1	O3	78.49(8)
O2	Co1	N1	100.18(9)
O2	Co1	N2	72.97(9)
O2	Co1	N3	117.06(9)
O2	Co1	N4	160.00(9)
O3	Co1	N1	76.91(9)
O3	Co1	N2	137.57(9)
O3	Co1	N3	146.09(9)
O3	Co1	N4	81.99(9)
N1	Co1	N2	78.00(9)

N1	Co1	N3	124.71(9)
N1	Co1	N4	79.4(1)
N2	Co1	N3	76.01(9)
N2	Co1	N4	125.76(9)
N3	Co1	N4	77.78(9)

Table S10. Selected bond angles (°) for the complex cation $[Co(DHP)]^{2+}$

Atom 1	Atom 2	Atom 3	Angle (°)
O1	Co1	O2	77.6(1)
O1	Co1	N1	76.8(1)
O1	Co1	N2	119.0(1)
O1	Co1	N3	149.8(1)
O1	Co1	N4	102.4(1)
O2	Co1	N1	150.3(1)
O2	Co1	N2	99.5(1)
O2	Co1	N3	76.0(1)
O2	Co1	N4	121.4(1)
N1	Co1	N2	80.2(1)
N1	Co1	N3	132.1(1)
N1	Co1	N4	78.9(1)
N2	Co1	N3	79.9(1)
N2	Co1	N4	127.2(1)
N3	Co1	N4	79.4(1)

Table S11. Selected bond angles (°) for the complex cation $[Co(THP)]^{2+}$

Atom 1	Atom 2	Atom 3	Angle (°)
O1	Co1	O2	77.4(1)
O1	Co1	O3	80.9(1)
O1	Co1	N1	74.0(1)

O1	Co1	N2	123.7(1)
O1	Co1	N3	155.9(1)
O1	Co1	N4	93.9(1)
O2	Co1	O3	74.9(1)
O2	Co1	N1	111.9(1)
O2	Co1	N2	70.3(1)
O2	Co1	N3	103.9(2)
O2	Co1	N4	163.5(1)
O3	Co1	N1	151.4(1)
O3	Co1	N2	129.7(1)
O3	Co1	N3	76.4(1)
O3	Co1	N4	90.0(1)
N1	Co1	N2	76.9(2)
N1	Co1	N3	125.4(2)
N1	Co1	N4	78.5(2)
N2	Co1	N3	78.1(2)
N2	Co1	N4	125.7(2)
N3	Co1	N4	78.2(2)

Table S12. Selected bond angles (°) for the complex cation $[Co(BABC)]^{2+}$

Atom 1	Atom 2	Atom 3	Angle (°)
O1	Co1	O2	77.07(4)
O1	Co1	N4	89.65(4)
O1	Co1	N2	106.36(4)
O1	Co1	N3	153.69(4)
O1	Co1	N1	77.76(4)
O2	Co1	N4	99.50(4)
O2	Co1	N2	95.99(4)

O2	Co1	N3	77.13(4)
O2	Co1	N1	154.77(4)
N4	Co1	N2	159.88(4)
N4	Co1	N3	89.56(4)
N4	Co1	N1	82.04(4)
N2	Co1	N3	81.43(4)
N2	Co1	N1	89.40(4)
N3	Co1	N1	128.10(4)

Additional Description of Structures.

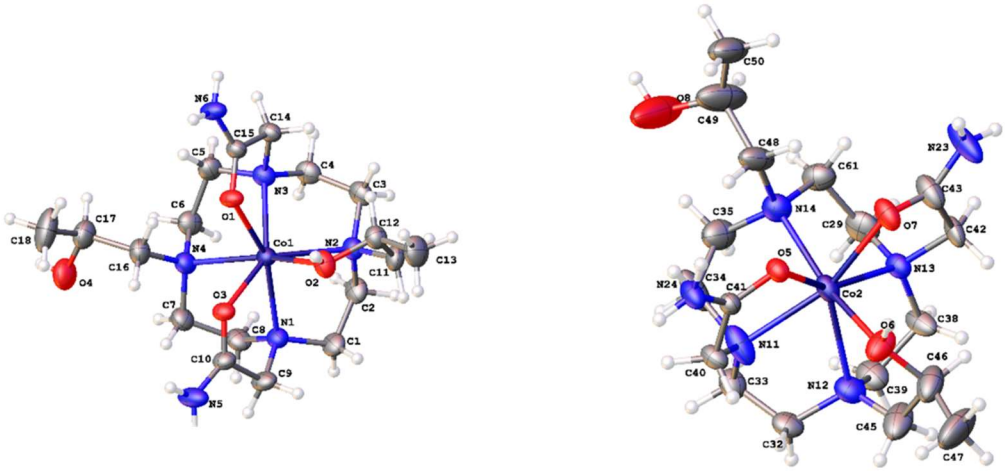

Figure S24. Two macrocyclic cations for $[Co(HPAC)]^{2+}$: For disordered cation (b) only one of components is shown. Thermal ellipsoids are drawn at 50% probability.

The coordination polyhedron of Co1 (and Co2) atom in the Co(II) complex of HPAC is a prismatoid with seven vertices with three oxygen atoms O1, O2, and O3 of pendant groups located in a upper trigonal face and four nitrogen atoms of 1,4,7,10-tetrazadodecane macrocycle form a rhombic lower face. The lower face is nearly planar, deviations of four nitrogen atoms from the mean plane are below 0.01 Å. Both faces can be considered parallel: the angle between two planes is 3.5(1)°; the distance between two faces is around 2.51 Å. Co1 atom is located 1.052(1) Å above mean plane of nitrogen atoms and 1.458 Å below the upper plane. Alternatively, the coordination polyhedron of Co atoms can be considered as a truncated rhombohedron with one vertex removed (Figure S22).

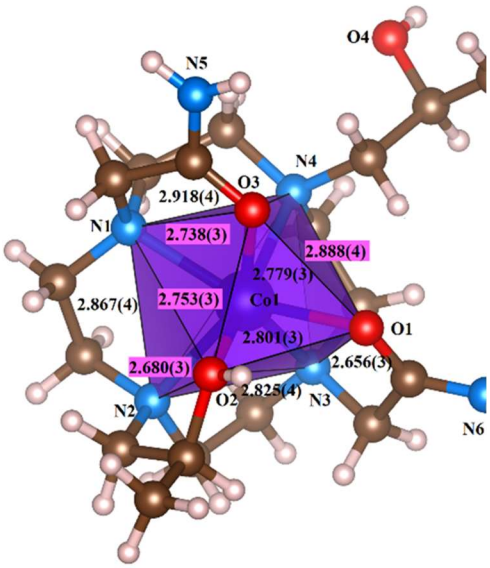

Figure S25. Coordination polyhedron of Co1 atom in the complex cation of $[Co(HPAC)]^{2+}$. Interatomic distances are shown in Å.

The structure of the Co(II) complex of DHP has the macrocyclic complex cation (Figure S23) and the tetrahedral tetrachloridocobaltate(II) anion. Coordination polyhedron of Co1 atom is a distorted wedge with six vertices with two oxygen atoms O1 and O2 of pendant groups located in *cis*- position above the plane of four nitrogen atoms.

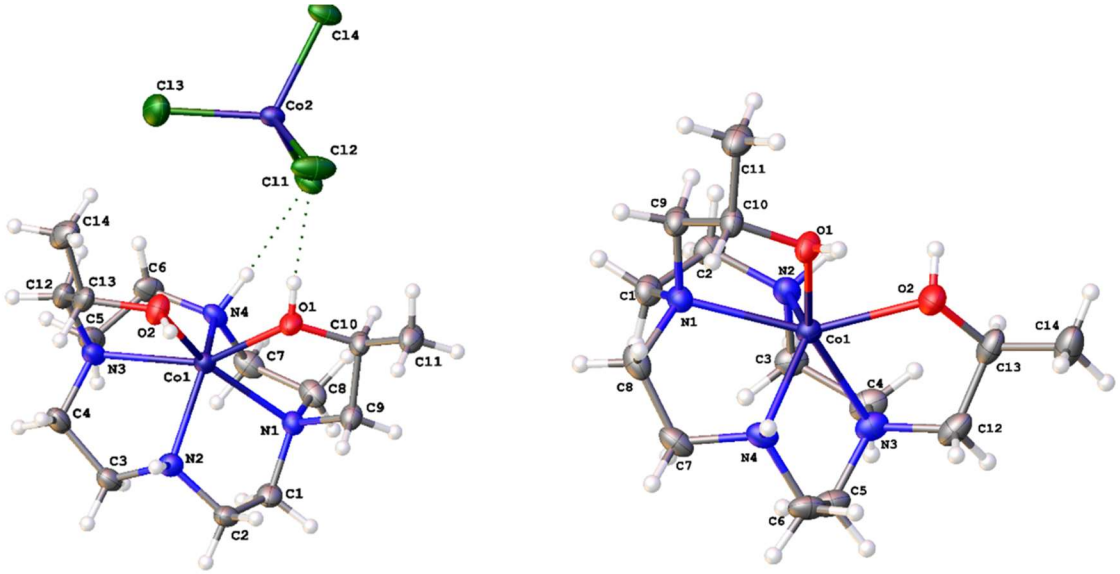

Figure S26. Numbering scheme for the Co(II) complex with DHP with thermal ellipsoids drawn at 50% probability.

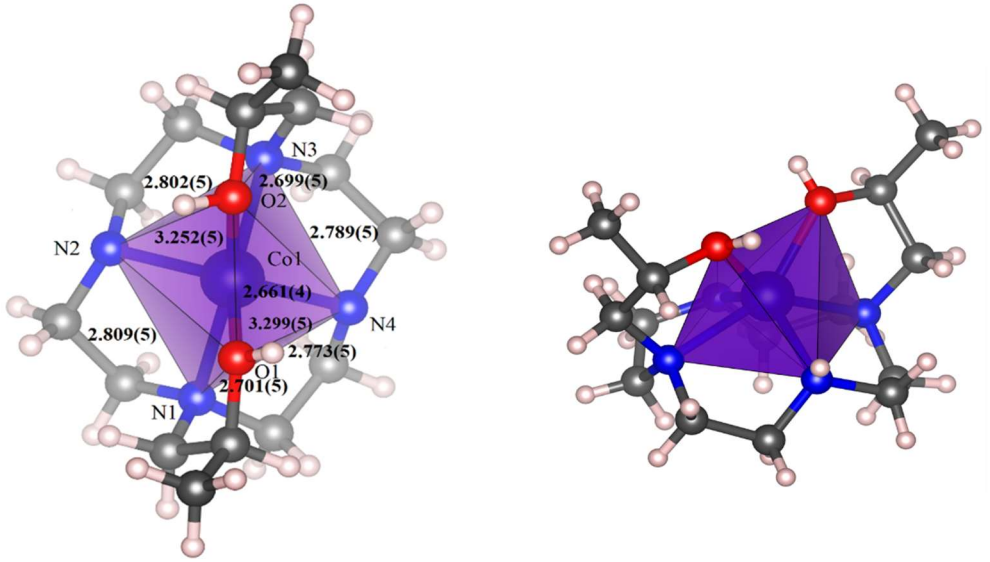

Figure S27. Coordination polyhedron of Co1 atom in the complex cation of $[Co(DHP)]^{2+}$. Interatomic distances are shown in Å.

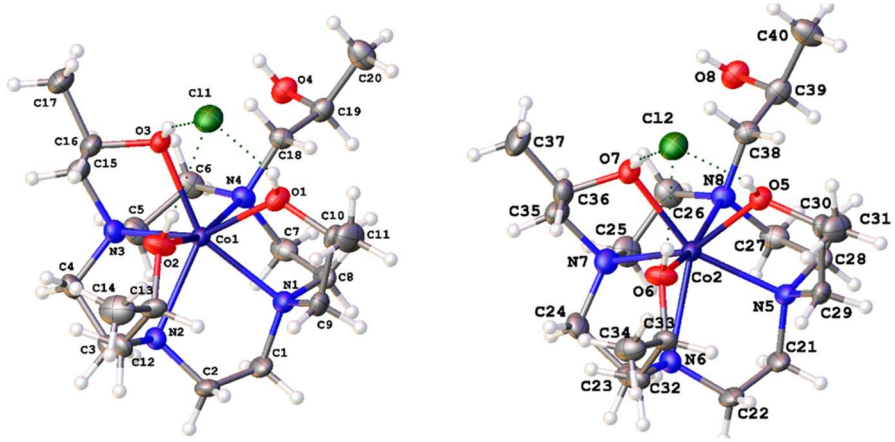

Figure S28. Molecular structure and numbering scheme of two macrocyclic cations for the Co(II) complex of THP. Thermal ellipsoids are drawn at 50% probability.

Asymmetric unit consists of two crystallographically independent macrocyclic complex cations of Co(THP), two chloride ions, a disordered tetrahedral tetrachloridocobaltate(II) anion, two water molecules, and an acetonitrile molecule. Both macrocyclic cations are similar (Figure S25).

The coordination polyhedra of Co1 and Co2 atoms are prismatoids with seven vertices with three oxygen atoms O1, O2, and O3 (and O5, O6 and O7) of pendant groups located in a upper trigonal face and four nitrogen atoms of 1,4,7,10-tetrazadodecane macrocycle form rhombic lower faces. The lower face is nearly planar; deviations of four nitrogen atoms from the mean plane are 0.02 Å (Co1) and 0.026 Å (Co2). Both triangular and rhombic faces can be considered parallel: the angle between two planes is 1.4(1)°for Co1 complex and 1.2° for Co2. Co1 atom is located

1.039(2) Å above mean plane of nitrogen atoms and 1.519(2) Å below the upper plane; Co2 atom is located 1.041(2) Å above mean plane of nitrogen atoms and 1.525(2) Å below the upper plane. Alternatively, the coordination polyhedra of Co atoms can be considered as truncated rhombohedra with one vertex removed. In both twelve-membered macrocycles, four C-N bonds have *trans*- conformation and four are *gauche*; all C-C bonds are *gauche*. The overall sequence is *(TGG)*$_4$. Another notation for this conformation is [3333] (Boyens & Dobson, 1987)[12]. See Figure S26.

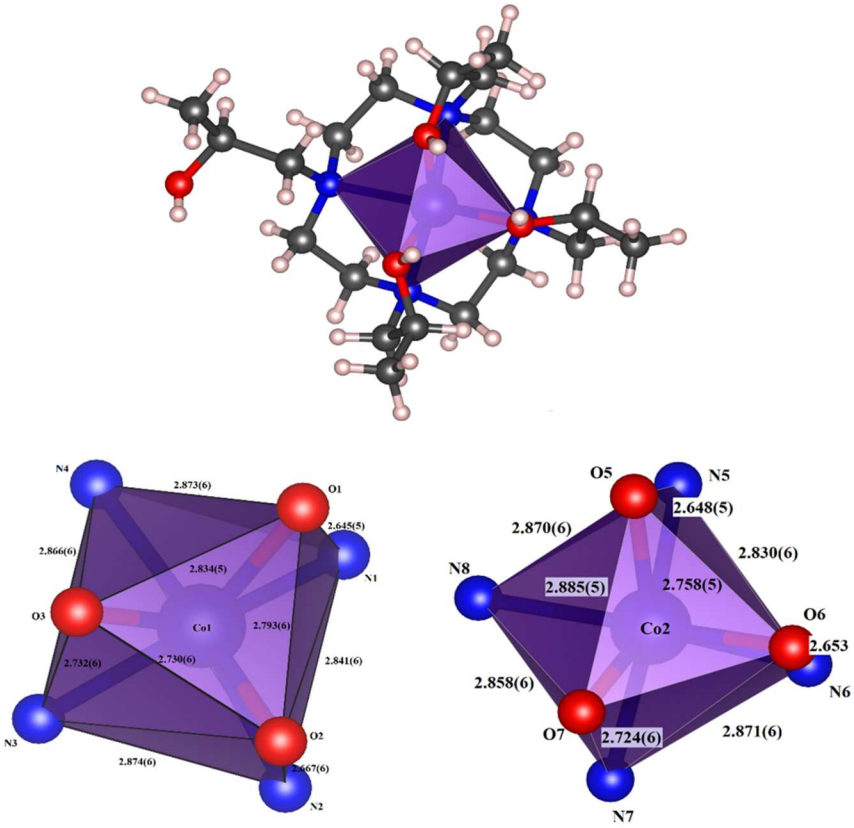

Figure S29. Coordination polyhedra of macrocyclic complex cations for $[Co(THP)]^{2+}$. Interatomic distances in Å.

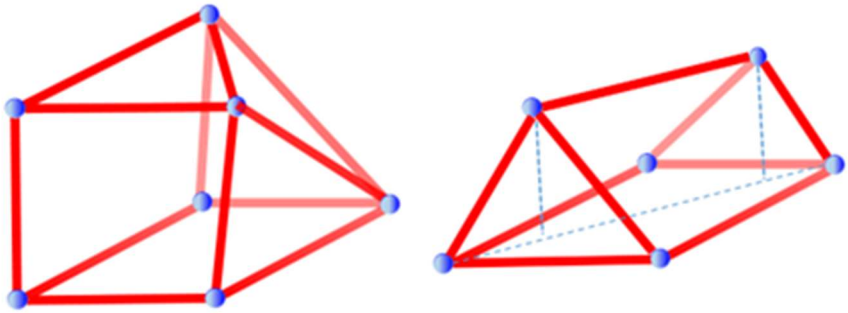

Figure S30. Prismatoid and distorted wedge geometries.

References.

(1) *SADABS v2014/5*; Bruker AXS Inc.: Madison, Wisconsin, USA., 2014.
(2) *SAINT v8.34A*; Bruker AXS Inc.: Madison, Wisconsin, USA, 2013.
(3) Sheldrick, G. SHELXT - Integrated space-group and crystal-structure determination. *Acta Crystallogr Section A* **2015**, *71* (1), 3-8.
(4) Sheldrick, G. Crystal structure refinement with SHELXL. *Acta Crystallogr Section C* **2015**, *71* (1), 3-8.
(5) Dolomanov, O. V.; Bourhis, L. J.; Gildea, R. J.; Howard, J. A. K.; Puschmann, H. OLEX2: a complete structure solution, refinement and analysis program. *J Appl Crystallogr* **2009**, *42* (2), 339-341. DOI: doi:10.1107/S0021889808042726.
(6) McGarvey, D. R. C., William R. *NMR METHOD TO DETERMINE NIST-TRACEABLE QUANTITATIVE WEIGHT PERCENTAGE PURITY OF NEAT AGENT T*; Edgewood Chemical Biological Center, Aberdeen Proving Ground, MD 21020-5424, 2018.
(7) Evans, D. F. 400. The determination of the paramagnetic susceptibility of substances in solution by nuclear magnetic resonance. *J Chem Soc* **1959**, 2003-2005, 10.1039/JR9590002003.
(8) Bain, G. A.; Berry, J. F. Diamagnetic Corrections and Pascal's Constants. *J Chem Ed* **2008**, *85* (4), 532.
(9) Rodríguez-Rodríguez, A.; Regueiro-Figueroa, M.; Esteban-Gómez, D.; Rodríguez-Blas, T.; Patinec, V.; Tripier, R.; Tircsó, G.; Carniato, F.; Botta, M.; Platas-Iglesias, C. Definition of the Labile Capping Bond Effect in Lanthanide Complexes. *Chem Eur J* **2017**, *23* (5), 1110-1117.
(10) Royal, G.; Dahaoui-Gindrey, V.; Dahaoui, S.; Tabard, A.; Guilard, R.; Pullumbi, P.; Lecomte, C. New Synthesis of trans-Disubstituted Cyclam Macrocycles – Elucidation of the Disubstitution Mechanism on the Basis of X-ray Data and Molecular Modeling. *Eur J Org Chem* **1998**, *1998* (9), 1971-1975.
(11) Parsons, S.; Flack, H. D.; Wagner, T. Use of intensity quotients and differences in absolute structure refinement. *Acta Crystallogr B Struct Sci Cryst Eng Mater* **2013**, *69* (Pt 3), 249-259.
(12) Hancock, R. D.; Dobson, S. M.; Boeyens, J. C. A. Metal ion size selectivity of 1-Thia-4, 7-diazacyclononane (9-aneN:S), and other tridentate macrocycles. A study by molecular mechanics calculation, structure determination, and formation constant determination of complexes of 9-aneN 2S. *Inorg Chim Acta* **1987**, *133* (2), 221-231.